⌘ *Author's Choice*

THE JOURNAL OF BIOLOGICAL CHEMISTRY VOL. 283, NO. 41, pp. 27426–27432, October 10, 2008

Identification of Pore Residues Engaged in Determining Divalent Cationic Permeation in Transient Receptor Potential Melastatin Subtype Channel 2*[S]

Received for publication, February 8, 2008, and in revised form, July 9, 2008 Published, JBC Papers in Press, August 7, 2008, DOI 10.1074/jbc.M801049200

Rong Xia[1], **Zhu-Zhong Mei, Hong-Ju Mao**[2], **Wei Yang**[3], **Li Dong**[4], **Helen Bradley, David J. Beech, and Lin-Hua Jiang**[5]

From the Institute of Membrane and Systems Biology, Faculty of Biological Sciences, University of Leeds, Leeds LS2 9JT, United Kingdom

The molecular basis for divalent cationic permeability in transient receptor potential melastatin subtype (TRPM) channels is not fully understood. Here we studied the roles of all eight acidic residues, glutamate or aspartate, and also the glutamine residue between pore helix and selectivity filter in the pore of TRPM2 channel. Mutants with alanine substitution in each of the acidic residues, except Glu-960 and Asp-987, formed functional channels. These channels exhibited similar Ca^{2+} and Mg^{2+} permeability to wild type channel, with the exception of the E1022A mutant, which displayed increased Mg^{2+} permeability. More conservative E960Q, E960D, and D987N mutations also led to loss of function. The D987E mutant was functional and showed greater Ca^{2+} permeability along with concentration-dependent inhibition of Na^{+}-carrying currents by Ca^{2+}. Incorporation of negative charge in place of Gln-981 between the pore helix and selectivity filter by changing it to glutamate, which is present in the more Ca^{2+}-permeable TRPM channels, substantially increased Ca^{2+} permeability. Expression of concatemers linking wild type and E960D mutant subunits resulted in functional channels that exhibited reduced Ca^{2+} permeability. These data taken together suggest that Glu-960, Gln-981, Asp-987, and Glu-1022 residues are engaged in determining divalent cationic permeation properties of the TRPM2 channel.

The melastatin subtype of transient receptor potential (TRPM)[6] ion channels is widely expressed in neuronal, cardiovascular, immune, and endothelial cells where they are engaged in diverse physiological and pathophysiological processes (1–7). TRPM2 channels are activated by adenosine diphosphoribose (ADPR) and also by oxidative stress and mediate immune function, insulin secretion, endothelial permeability, and cell death that are induced by oxidative stress (8–14).

All members of the transient receptor potential (TRP) channel superfamily, which includes TRPC, TRPV, TRPM, TRPP, TRPML, and TRPA subfamilies, have a basic architecture similar to voltage-gated potassium channels, with homo- or hetero-tetrameric arrangements around a central ion-conducting pore (1, 7, 15). Each subunit is considered to have intracellular N and C termini and six transmembrane segments (S1–S6) with a re-entrant pore loop connecting S5 and S6 (see Fig. 1*A*). Despite significant differences in the amino acid residue sequences of the pore loop among different TRP subfamilies, there are two stretches of amino acid residues that are thought to form the pore helix and the ion selectivity filter of these channels, respectively (15).

TRPM channels, including TRPM2, show considerable permeability to Ca^{2+} and other divalent cations, with the exception of TRPM4/5 channels that are selective for monovalent cations (8, 9, 13–18). The molecular basis for divalent cationic permeability of TRPM channels is not fully understood. Accumulating evidence supports an important role of the ion selectivity filter in Ca^{2+} and Mg^{2+} permeation of TRPV and TRPM channels (15, 19–26). A consistent feature is conserved acidic or negatively charged residues in the selective filter. Such residues are determinants of selective permeation to cations, especially Ca^{2+}, in several ion channels (15, 27, 28). Indeed these residues are recognized to be important in TRPV channels (19–21); however, their role in TRPM channels is less clear. Alanine substitution in TRPM4 (D984A) or TRPM6 (D1031A) leads to loss of function (22, 25). In contrast, the TRPM7 channel carrying the D1054A mutation is functional and has virtually the same pore properties as wild type (WT), including the Ca^{2+} and Mg^{2+} permeation (23). Neutralization of Glu-1029 in TRPM6 or Glu-1052 in TRPM7 in the linker region between the pore helix and the selective filter significantly reduces Ca^{2+} and Mg^{2+} permeability. Conversely, incorporation of negative charge to the equivalent Gln-977 in TRPM4 or Gln-914 in TRPM8 substantially increases Ca^{2+} permeability (22–24).

Here we examined all the acidic pore residues and additionally Gln-981 in the linker region of TRPM2 channel (see Fig. 1*A*). We found that the residues Glu-960, Gln-981, and Asp-

* This work was supported by the Wellcome Trust (to L.-H. Jiang). The costs of publication of this article were defrayed in part by the payment of page charges. This article must therefore be hereby marked "*advertisement*" in accordance with 18 U.S.C. Section 1734 solely to indicate this fact.

⌘ *Author's Choice*—Final version full access.

[S] The on-line version of this article (available at http://www.jbc.org) contains five supplemental figures.

[1] A recipient of the UK Overseas Research Scholarship.

[2] A Royal Society visiting research fellow from the Shanghai Institute of Microsystems and Information Technology, Chinese Academy of Science, China.

[3] A visiting scholar from the School of Medicine, Zhejiang University, China. Supported in part by a Worldwide Universities Network global exchange award.

[4] A visiting scholar from and supported by School of Medicine, Shanghai Jiaotong University, China.

[5] To whom correspondence should be addressed. E-mail:: l.h.jiang@leeds.ac.uk.

[6] The abbreviations used are: TRP, transient receptor potential; TRPM, transient receptor potential melastatin subtype; WT, wild type; ADPR, adenosine diphosphoribose.

TABLE 1
Compositions of extracellular recording solutions (in mM)

	Solutions					
	NaCl	KCl	$MgCl_2$	$CaCl_2$	HEPES	Glucose
Standard	147	2	1	2	10	13
147 NaCl + 2 $CaCl_2$ + 1 $MgCl_2$	147	0	1	2	10	13
147 NaCl (no $CaCl_2$)	147	0	0	0	10	24
147 NaCl + 0.1 $CaCl_2$	147	0	0	0.1	10	24
147 NaCl + 0.3 $CaCl_2$	147	0	0	0.3	10	22
147 NaCl + 1 $CaCl_2$	147	0	0	1	10	21
147 NaCl + 2 $CaCl_2$	147	0	0	2	10	17
147 NaCl + 3 $CaCl_2$	147	0	0	3	10	11
147 NaCl + 10 $CaCl_2$	147	0	0	10	10	0
147 NaCl + 2 $MgCl_2$	147	0	2	0	10	20
110 $CaCl_2$	0	0	0	110	10	24
110 $MgCl_2$	0	0	110	0	10	24

987 contribute significantly to defining Ca^{2+} permeation and Glu-1022 to Mg^{2+} permeation of the TRPM2 channel.

EXPERIMENTAL PROCEDURES

Constructs, Cell Culture, and Transfection—The construct encoding human TRPM2 (8) with a C-terminal EE epitope (29) was used. Mutations were introduced using QuikChange system (Stratagene) and confirmed by sequencing. The constructs encoding subunit concatemers with a C-terminal EE epitope were made as follows. Firstly, the sequence (nucleotides 1–700) encoding part of the TRPM2 N terminus (TRPM2N) was amplified by PCR using *Pfu* and forward primer 5′-TCTCT-AGA*ATGGAGCCCTCAGCCCTGAGG*-3′ (XbaI sequence underlined and TRPM2 sequence in italic) and reverse primer 5′-TCAGTACAGGTAGAGCAAGGTGTCC-3′. The resultant PCR product containing XbaI site was inserted into pCR2.1 following the manufacturer's instructions (Invitrogen) to generate TRPM2N-pCR2.1. Secondly, the vector sequence between EcoRI and XbaI and the TRPM2 sequence between XbaI and SacI were separately excised from TRPM2N-pCR2.1 and ligated with the sequence between SacI and EcoRI from TRPM2-EE-pcDNA3.1 to generate TRPM2-EE-pCR2.1. Finally, the TRPM2-EE sequence between XbaI and HindIII was excised from TRPM2-EE-pCR2.1 to replace the sequence between XbaI and PmeI in TRPM2-Myc-pcDNA3.1 to produce the constructs encoding concatenated subunits (see Fig. 4*A*). Maintenance of human embryonic kidney cells (HEK293) and transient transfection with plasmids were described previously (29).

Biotin Labeling and Western Blotting Analysis—Experiments were performed as described previously (29, 30). Proteins were resolved on SDS-PAGE gels and detected using primary rabbit anti-EE antibody (1:2000 dilution; Bethyl Laboratories) and secondary goat horseradish peroxidase-conjugated anti-rabbit IgG antibody (1:2000 dilution; Santa Cruz Biotechnology).

Electrophysiological Recording—Whole-cell recordings were made using an Axopatch 200B amplifier at room temperature 24–48 h after transfection as described previously (29, 30). The data were filtered at 2 kHz and sampled at 10 kHz. Cells were held at −40 mV and voltage ramps with a 1-s duration from −120 mV to 80 mV were applied every 5 s. The currents at −80 mV denoted in the figures by *circles* (see Figs. 1, *B* and *C*, 3, *A–D*, and 4, *C* and *D*) were obtained from the current responses to voltage ramps. In some experiments, cells were held constantly at −40 mV or 40 mV, and the currents were plotted as continuous lines (see Fig. 3*E*). Intracellular solution contained (in mM): 147 NaCl, 0.05 EGTA, 1 $MgCl_2$, 10 HEPES, 1 Na_2ATP, and 1 ADPR. Table 1 lists the compositions of extracellular solutions used. Flufenamic acid (FFA) (0.5 mM) (31) or *N*-(p-amylcinnamoyl) anthranilic acid (20 μM) (32) was applied at the end of each recording via a RSC-160 system (Biologic Science Instruments) to confirm TRPM2 channel-mediated currents.

The reversal or zero-current potentials (E_r) were determined from current responses to the aforementioned voltage ramps. After cell-attached configuration was established in standard extracellular solution, application of voltage ramps started and continued throughout experiments, during which whole-cell configuration was achieved at least 2 min after the external solution was replaced with the indicated extracellular solutions. The flufenamic acid/anthranilic acid-insensitive current components were negligible (*e.g.* Fig. 1*B*), and no subtraction from the total currents was made. The reversal potentials were corrected for liquid junction potentials as we described previously (33). Ion activities were used, converted from ion concentrations using the following coefficients: $\gamma_{Na} = 0.75$, $\gamma_{Ca} = 0.28$, and $\gamma_{Mg} = 0.34$. The relative permeability P_X/P_{Na} (X = calcium or magnesium) were derived using the Goldman-Hodgkin-Katz equation (8, 23): $P_X/P_{Na} = [Na]_i \exp(E_rF/RT)\ (1 + \exp(E_rF/RT))/4[X]_o$, where F, R, and T are Faraday constant, gas constant, and absolute temperature.

Data Analysis—All the data, where appropriate, are presented as mean ± S.E. The calcium inhibition was estimated by fitting to the Hill equation: I/I (%) = (100 − C)/[1+ ([calcium]/IC_{50})^n], where I is the sustained current as a percentage of the peak current (I_p), C is the Ca^{2+}-insensitive current component, IC_{50} is the concentration producing half-maximal inhibition, and n is the Hill coefficient. Curve fitting was carried using Origin (OriginLab, Northampton, MA). Comparisons were made using the Student's t test between two groups or analysis of variance (post hoc Tukey) between multiple groups with significance at the level of $p < 0.05$.

RESULTS

Effects of Mutating Acidic Pore Residues on Functional Channel Expression—Cells expressing WT TRPM2 channels responded to a supramaximal concentration of intracellular ADPR (1 mM) with robust currents that exhibited typical linear I/V relationship (Fig. 1*B*), as reported previously (29, 30). Expression of D1002A and E1010A mutants yielded current responses and I/V relationships that were virtually the same as WT (Fig. 1, *B* and *C*). D964A, E994A, and D1012A mutants showed similar currents (Fig. 1*C*) and I/V relationships (data not shown). There were no currents in cells expressing E960A and D987A mutants. Currents for the E1022A mutant were significantly reduced when compared with WT (Fig. 1*C*) despite normal surface expression shown by biotin-labeling analysis (supplemental Fig. 1).

We made further substitutions at positions 960 and 987 (Fig. 1*C*). Although the charge-conserving mutation E960D led to complete loss of function, D987E was functional, albeit the currents being slightly smaller. Channel function was abolished by

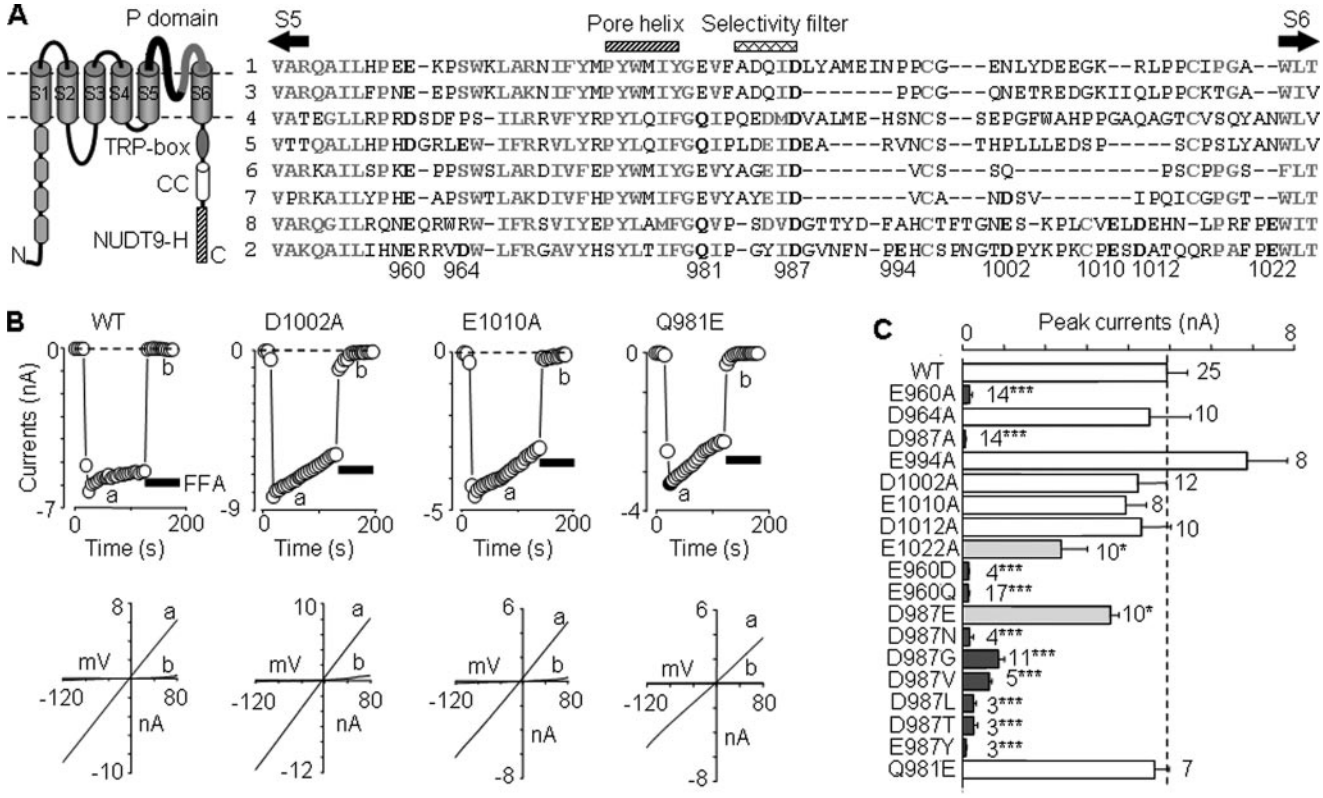

FIGURE 1. **Effects of mutating pore residues on functional channel expression.** *A*, *left*, schematic presentation of membrane topology of the TRPM2 subunit. It contains six transmembrane segments (S1–S6) with a pore loop between S5 and S6, four TRPM homology domains in the N terminus (*N*), and a stretch of highly conserved residues (*TRP-box*), a coiled-coil (*CC*) domain and NUTD9 homology (*NUTD9-H*) domain in the C terminus (*C*). *Right*, amino acid sequence alignment of human TRPM1–8 pore loops using ClustalW. The highly conserved residues are highlighted in *bold* and *gray*, and the residues in TRPM2 examined in this study (numbering according to hTRPM2) and those conserved in other TRPM subunits are in *bold* and *black*. *B*, representative ADPR-evoked currents at −80 mV (*top*, denoted by *circles*) and I/V curves (*bottom*), obtained by voltage ramps applied every 5 s, from cells expressing the WT or indicated mutant channels. The *horizontal bars* here and in the other figures represent application of flufenamic acid (0.5 mM; *black bars*) or anthranilic acid (20 μM; *hatched bars*). *C*, summary of the ADPR-evoked peak currents in cells expressing the WT or indicated mutant channels. The *dotted line* shows the mean current for the WT channel. The number of cells examined in each case is indicated. *, $p < 0.05$, and ***, $p < 0.001$, when compared with WT.

charge neutralization of Glu-960 or Asp-987 by substitution with other residues (Fig. 1*C*).

Effects of Mutating Acidic Pore Residues on Ca^{2+} and Mg^{2+} Permeability—We next examined Ca^{2+} and Mg^{2+} permeability relative to Na^+ permeability of WT and functional mutant channels. The results are summarized in Fig. 2. The WT channel showed substantial permeation to both Ca^{2+} and Mg^{2+} ($P_{Ca}/P_{Na} \sim 0.9$ and $P_{Mg}/P_{Na} \sim 0.5$), as described previously (8, 9, 13, 14, 24). All the functional alanine mutants, except E1022A, displayed similar Ca^{2+} and Mg^{2+} permeability to WT. E1022A mutation resulted in doubling of the Mg^{2+} permeability with no change in the Ca^{2+} permeability. In contrast, D987E mutation conferred significant increase in the Ca^{2+} permeability with no effect on the Mg^{2+} permeability. These data suggest that Glu-1022 and Asp-987 have distinct roles in the Mg^{2+} and Ca^{2+} permeation of the TRPM2 channel.

An Additional Residue Differentially Influencing Ca^{2+} and Mg^{2+} Permeability—We also examined the role of Gln-981 located in the linker region of the TRPM2 channel. This residue is also present in TRPM4/5/8 channels but is replaced with glutamate in the more Ca^{2+}-permeable TRPM1/3/6/7 channels (Fig. 1*A*). Q981E mutant was functional (Fig. 1, *B* and *C*) and exhibited significant increase in the Ca^{2+} permeability with no change in the Mg^{2+} permeability (Fig. 2).

Ca^{2+} Inhibition of Na^+-carrying Currents of D987E Mutant—Unlike the sustained currents observed at WT, the currents for D987E mutant were transient in extracellular solution containing Na^+ as the major cation and low concentrations of Ca^{2+} and Mg^{2+} (Fig. 3*A*). In the absence of Ca^{2+}, the currents for both WT and D987E mutant were stable but considerably smaller (supplemental Fig. 2), likely reflecting the lack of Ca^{2+}-dependent facilitation (34, 35). In the presence of extracellular Ca^{2+} (but absence of Mg^{2+}), the currents for D987E mutant were large and also declined. The current decline was, however, readily reversed upon the subsequent removal of extracellular Ca^{2+} (Fig. 3*B*), suggesting that the current decline primarily results from the inhibition rather than desensitization of the ion-conducting channels. Further analysis showed that the current inhibition by Ca^{2+} was concentration-dependent, with an IC_{50} of 580 μM and a Hill coefficient of 1.7 (Fig. 3, *C* and *D*). We also measured currents in isotonic $CaCl_2$ solution. Currents carried by Ca^{2+} were largely sustained for WT but diminished rapidly for D987E mutant (supplemental Fig. 3).

To explore whether the current inhibition by Ca^{2+} resulted from entry of extracellular Ca^{2+} into the pore, we measured Na^+

outward currents at +40 mV to prevent extracellular Ca^{2+} from entering the pore. We also measured Na^+ inward currents at −40 mV, when extracellular Ca^{2+} can readily enter the pore. As illustrated in Fig. 3*E*, the outward currents at +40 mV showed minimal decline, whereas the inward currents at −40 mV were transient.

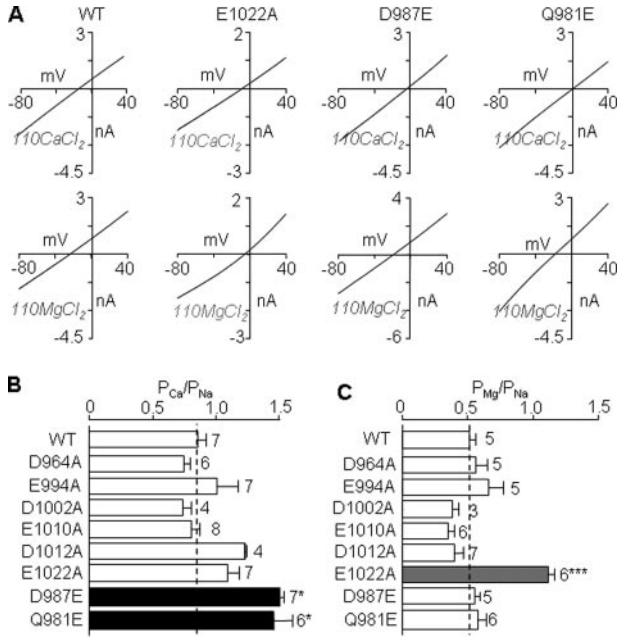

FIGURE 2. **Mutational effects on the Ca^{2+} and Mg^{2+} permeability.** *A*, representative I/V curves in extracellular 110 mM $CaCl_2$ (*top*) or 110 mM $MgCl_2$ solution (*bottom*) for the WT, E1022A, D987E, or Q981E mutant channels. *B* and *C*, summary of the P_{Ca}/P_{Na} (*B*) and P_{Mg}/P_{Na} (*C*), derived from reversal potentials determined from the I/V curves shown in *A*, for all the channels examined. The *dotted lines* show the mean values for the WT channel. The number of cells examined in each case is indicated. *, $p < 0.05$, and ***, $p < 0.001$, when compared with WT.

Ca^{2+} and Mg^{2+} Permeability of Subunit Concatemer Channels—Loss of channel function resulting from mutation of Glu-960 (E960D/Q) and Asp-987 (D987N) prevented us from further studying the role of these two highly conserved residues in Ca^{2+} and Mg^{2+} permeation of TRPM2 channel. In an effort to overcome the difficulty, we concatenated WT and mutant subunits (WT-E960D, WT-E960Q, and WT-D987N) (Fig. 4*A*) and sought to express functional channels comprising WT and mutant subunits. We also made WT-WT and WT-D987E concatemers. As shown by Western blotting, the protein expression was similar among the concatemers but significantly lower when compared with WT or mutant subunit alone (Fig. 4*B*). Expression of all the concatemers, except WT-E960Q, resulted in ADPR-evoked currents with typical linear I/V (Fig. 4, *C* and *D*). The same results were obtained with concatemers in which mutations were introduced in the first subunit (E960D-WT, E960Q-WT, and D987N-WT) (Fig. 4*D*). Taken together, these data suggest that both WT and mutant subunits contribute to the channel assembly. Furthermore, the WT-WT concatemer exhibited the same Ca^{2+} and Mg^{2+} permeability as WT (Fig. 5*C*), providing functional evidence indicating that subunit concatenation imposes negligible constraints affecting the ion-conducting pore.

The concatemers containing D987E mutant subunit (WT-D987E and D987E-WT) were more permeable to Ca^{2+} than WT-WT, consistent with the idea that D987E mutation increased the Ca^{2+} permeability. However, the concatemers having D987N mutant subunit (WT-D987N and D987N-WT) displayed similar Ca^{2+} permeability to WT-WT (Fig. 5*B*). These contrasting data support the notion that the side-chain length of residue at position 987 influences the Ca^{2+} permeation. Most interestingly, the concatemers containing E960D mutant subunit (WT-E960D and E960D-WT) became significantly less Ca^{2+}-permeable (Fig. 5*B*), indicating that E960D mutation reduced the Ca^{2+} permeability.

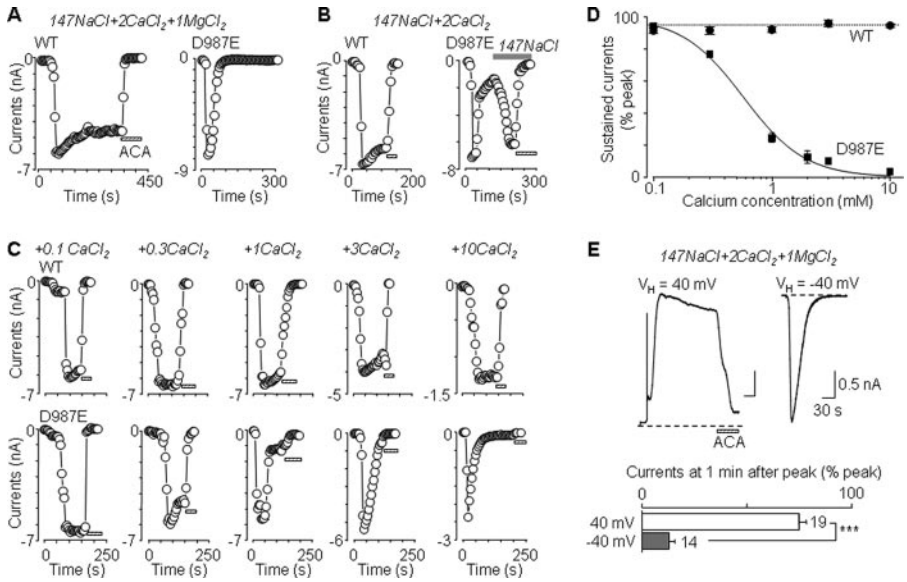

FIGURE 3. **D987E mutation confers concentration-dependent inhibition of Na^+-carrying currents by Ca^{2+}.** *A–C*, representative ADPR-evoked currents at −80 mV (denoted by *circles*), obtained by voltage ramps every 5 s, from cells expressing the WT or D987E mutant channels in extracellular 147 mM NaCl solution containing 2 mM $CaCl_2$ and 1 mM $MgCl_2$ (*A*), 2 mM $CaCl_2$ (*B*), or $CaCl_2$ at the indicated concentrations (*C*). *D*, summary of the sustained currents expressed as a percentage of the peak currents. The *smooth line* for the D987E mutant channel represents the curve fit to the Hill equation ($IC_{50} = 580\ \mu M$ and $n = 1.7$). $n = 4–7$ cells for each data point. *E*, *top*, representative ADPR-evoked currents in cells expressing the D987E mutant channel with membrane potentials being constantly held at 40 and −40 mV, respectively. *Bottom*, summary of the sustained currents at 50 s after reaching the peak, expressed as a percentage of the peak currents. The number of cells examined in each case is indicated. ***, $p < 0.001$ between inward and outward currents.

DISCUSSION

Glu-960 and Asp-987 Are Important for Functional Expression of TRPM2 Channel—Charge-conserving or charge-neutralizing mutation of Glu-960 prevented channel function (Fig. 1), despite negligible effects on total and membrane protein expression (supplemental Fig. 1). Loss of function resulting from the E960D mutation is intriguing, considering the fact

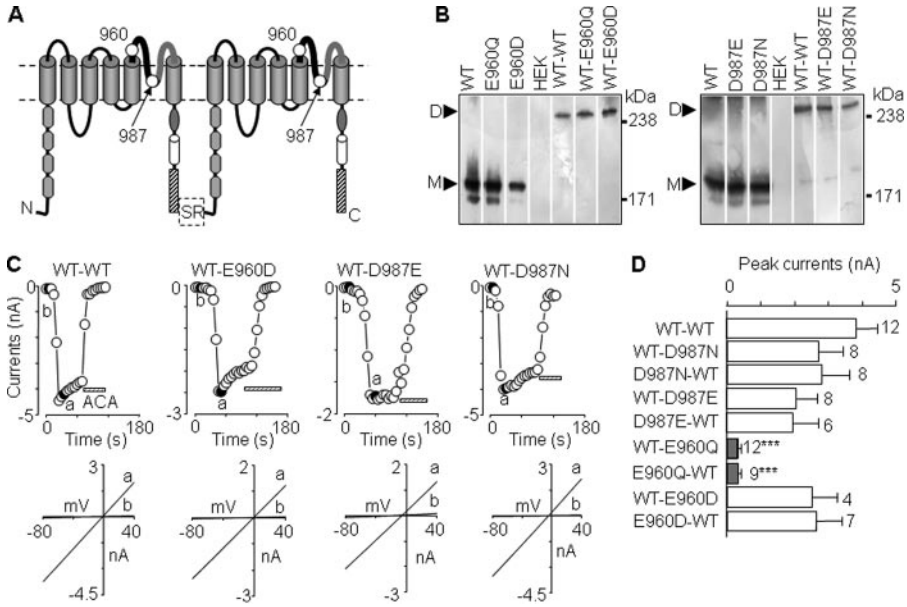

FIGURE 4. **Construction and expression of TRPM2 subunit concatemers.** *A*, schematic diagram of TRPM2 subunit concatenation. The linker consists of serine and arginine (*SR*) residues. Position 960 was glutamate (WT), glutamine (E960Q mutant), or aspartate (E960D mutant), and position 987 was aspartate (WT), asparagine (D987N mutant), or glutamate (D987E mutant). *N*, N terminus; *C*, C terminus. *B*, Western blotting analysis of protein expression of the indicated subunits and subunit concatemers. The proteins were immunoprecipitated and detected by an anti-EE antibody. The *arrowheads* denote the expected monomeric (*M*) and dimeric proteins (*D*), respectively. *C*, representative ADPR-evoked currents at −80 mV (denoted by *circles*, *top*) and I/V curves (*bottom*), obtained by voltage ramps applied every 5 s, from cells expressing the indicated subunit concatemers. *ACA*, anthranilic acid. *D*, summary of the ADPR-evoked peak currents in cells expressing the indicated subunit concatemers. The number of cells examined in each case is indicated. ***, $p < 0.001$, when compared with WT-WT.

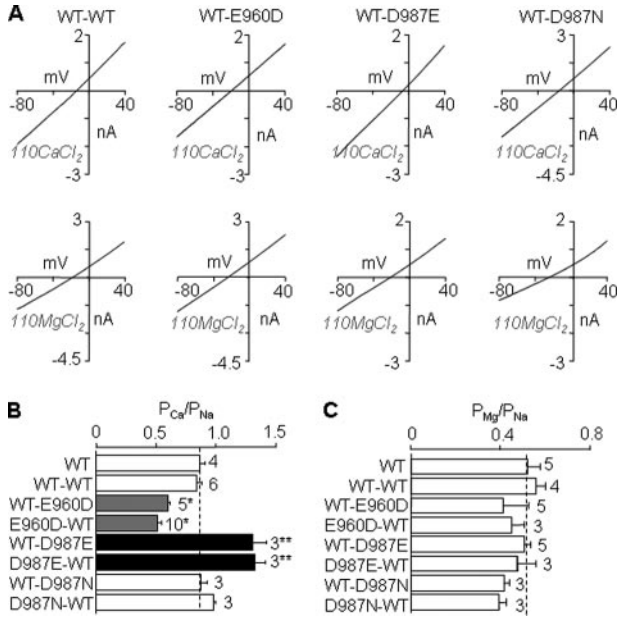

FIGURE 5. **Ca^{2+} and Mg^{2+} permeability of functional subunit concatemers.** *A*, representative I/V curves from cells expressing the indicated concatemers in extracellular 110 mM $CaCl_2$ (*top*) or 110 mM $MgCl_2$ solution (*bottom*). *B* and *C*, summary of the P_{Ca}/P_{Na} (*B*) and P_{Mg}/P_{Na} (*C*), derived from reversal potentials measured from the I-V curves shown in *A*, for all the subunit concatemers examined. The *dotted lines* show the mean values for the WT channel. The number of cells examined in each case is indicated. *, $p < 0.05$, and **, $p < 0.01$, when compared with WT-WT concatemer and WT.

that aspartate is present in the corresponding position of TRPM4/5 channels. The exact reasons are unclear and could relate to subtle differences in the local structure due to adjacent residues including proline (Fig. 1*A*). Moreover, the WT-E960D but not WT-E960Q concatemer formed functional channels. Such differentiating results suggest that glutamate at this position and particularly its negative charge are vital for functional expression of TRPM2 channel.

As for Glu-960, alanine substitution of Asp-987 had no effect on cell surface expression and yet imparted functional lethality (Fig. 1 and supplemental Fig. 1). These results are comparable with those reported in studies of Asp-984 in TRPM4 (22) and Asp-1031 in TRPM6 (25) but differ from those of Asp-1052 in TRPM7 (23). We further demonstrate that substitution of Asp-987 with several other residues, except negatively charged glutamate, also resulted in loss of function (Fig. 1*C*). Thus the results from present and previous studies indicate that aspartate at this position is important for functional expression of TRPM2/4/6 channels.

Glu-960, Asp-987, and Gln-981 as Determinants of Ca^{2+} Permeability—Glu-960, or its equivalent, is conserved in Ca^{2+}-permeable TRPM channels but is replaced by aspartate in the Ca^{2+}-impermeable TRPM4/5 channels (Fig. 1*A*). Thus it would be informative if the E960D mutant were functional. Although it was not, we adopted the subunit concatenation strategy and showed that the concatemer channels carrying the E960D mutation (WT-E960D and E960D-WT) exhibited reduced Ca^{2+} permeability (Fig. 5), consistent with a significant role of Glu-960 or the equivalent residue in defining the Ca^{2+} permeation of TRPM channels.

Glu-960 is close to the extracellular end of S5 and therefore is possibly situated on the wide external pore vestibule (15). Previous studies have identified residues in this microdomain that interact with and mediate functional modulation of TRP channels by extracellular cations. These include Glu-543 in potentiation of TRPC5 by La^{3+} and H^+ (36, 37), Glu-600 in facilitation of TRPV1 by H^+ (38), and His-896 in recovery from H^+-enhanced inactivation of TRPM5 (39). Glu-960 may also directly interact with extracellular Ca^{2+}. E960D mutation shortens the side chain by one CH_2 group and may, for this reason, reduce its interaction with Ca^{2+}.

Asp-987 is the only fully conserved negatively charged residue in the ion-selective filter of TRPM channels and also the only negatively charged residue in the ion-selective filter of TRPM2 channel (Fig. 1*A*). The ion-selective filter is located at the narrow part of the ion-conducting pathway and is known to play a major role in the ion-selective permeation of TRPV and TRPM channels (15). However, the role of the

conserved aspartate residue in the Ca^{2+} and Mg^{2+} permeation of TRPM channels has not been demonstrated due to difficulties associated with loss of function by alanine substitution (22, 25) (Fig. 1*C*). We have shown here that functional D987E mutant exhibited significantly increased Ca^{2+} permeability (Fig. 2*B*). The D987E mutation also conferred concentration-dependent inhibition of Na^+ currents by Ca^{2+}. The inhibition was reversed by removing extracellular Ca^{2+} (Fig. 3*B*) or prevented by a positive membrane potential (Fig. 3*E*). The simplest interpretation is that Asp-987 interacts with permeant Ca^{2+} and that the D987E mutation, which lengthens the side chain, enhances the interaction with Ca^{2+} by extending the negative charge further into the ion-conducting pathway. Such an interpretation is supported by the findings that the WT-D987E but not WT-D987N concatemer showed increased Ca^{2+} permeability and Ca^{2+} inhibition of Na^+ currents (Fig. 5 and supplemental Fig. 5). Lack of effects on Ca^{2+} permeability and Ca^{2+} inhibition of Na^+ currents for the WT-D987N concatemer, however, should not be taken as evidence against the importance of the negative charge of Asp-987 because the concatemer channels still carry two WT subunits that may suffice to retain the ion permeation properties.

TRPM2/4/5/8 channels contain glutamine (position 981 in TRPM2) in the linker region between the pore helix and the ion-selective filter; it is replaced with glutamate in other TRPM channels that are more permeable to Ca^{2+} (Fig. 1*A*). As expected, the Q981E mutation significantly enhanced the Ca^{2+} permeability (Fig. 2*C*) (24). Similarly, substitution with glutamate of Gln-977 in TRPM4 or Gln-914 in TRPM8 increases the Ca^{2+} permeability, whereas neutralization of the corresponding Glu-1029 in TRPM6 or Glu-1052 in TRPM7 decreases the Ca^{2+} permeability (22–24). These results strongly support that this position also contributes significantly to defining the Ca^{2+} permeation property of TRPM channels.

Glu-1022 as a Determinant of Mg^{2+} Permeability—With the exception of TRPM4/5, TRPM channels are also permeable to Mg^{2+} (13, 23, 24, 26) (Fig. 2). Here we observed no change in the Mg^{2+} permeability in any of the TRPM2 mutant channels except E1022A (Fig. 2). Like Q981E mutation in TRPM2, Q914E mutation in TRPM8 had no effect on the Mg^{2+} permeability despite significant increase in the Ca^{2+} permeability (24). One possible explanation is that permeation of Ca^{2+} and Mg^{2+} engages distinct and yet overlapping sets of residues. This notion is consistent with the finding that E1022A mutation only increased the Mg^{2+} permeability (Fig. 2*D*).

In summary, we have provided evidence that three pore residues (Glu-960, Gln-981, and Asp-987) contribute significantly to defining the Ca^{2+} permeation of TRPM2 channel, and a fourth residue (Glu-1022) contributes to Mg^{2+} permeation. Combined with results from previous studies (18–26), our data indicate that both conserved and channel-specific residues in the pore domain together determine the selective cationic permeation properties of the TRPM channels.

Acknowledgment—We are grateful to Dr A. M. Scharenberg (Washington University, Seattle, WA) for providing the human TRPM2 cDNA clone.

REFERENCES

1. Clapham, D. E. (2003) *Nature* **426,** 517–524
2. Perraud, A. L., Schmitz, C., and Scharenberg, A. M. (2003) *Cell Calcium* **33,** 519–531
3. Fleig, A., and Penner, R. (2004) *Trends Pharmacol. Sci.* **25,** 633–639
4. Hoenderop, J. G., and Bindels, R. J. (2005) *J. Am. Soc. Nephrol.* **16,** 15–26
5. Inoue, R., Jensen, L. J., Shi, J., Morita, H., Nishida, M., Honda, A., and Ito, Y. (2006) *Circ. Res.* **99,** 119–131
6. Nilius, B., Owsianik, G., Voets, T., and Peters, J. A. (2007) *Physiol. Rev.* **87,** 165–217
7. Venkatachalam, K., and Montell, C. (2007) *Annu. Rev. Biochem.* **76,** 387–417
8. Perraud, A. L., Fleig, A., Dunn, C. A., Bagley, L. A., Launay, P., Schmitz, C., Stokes, A. J., Zhu, Q., Bessman, M. J., Penner, R., Kinet, J. P., and Scharenberg, A. M. (2001) *Nature* **411,** 595–599
9. Sano, Y., Inamura, K., Miyake, A., Mochizuki, S., Yokoi, H., Matsushime, H., and Furuichi, K. (2001) *Science* **293,** 1270–1271
10. Hara, Y., Wakamori, M., Ishii, M., Maeno, E., Nishida, M., Yoshida, T., Yamada, H., Shimizu, S., Mori, E., Kudoh, J., Shimizu, N., Kurose, H., Okada, Y., Imoto, K., and Mori, Y. (2002) *Mol. Cell* **9,** 163–173
11. Zhang, W., Chu, X., Tong, Q., Cheung, J. Y., Conrad, K., Masker, K., and Miller, B. A. (2003) *J. Biol. Chem.* **278,** 16222–16229
12. Fonfria, E., Marshall, I. C., Boyfield, I., Skaper, S. D., Hughes, J. P., Owen, D. E., Zhang, W., Miller, B. A., Benham, C. D., and McNulty, S. (2005) *J. Neurochem.* **95,** 715–723
13. Togashi, K., Hara, Y., Tominaga, T., Higashi, T., Konishi, Y., Mori, Y., and Tominaga, M. (2006) *EMBO J.* **25,** 1804–1815
14. Hecquet, C. M., Ahmmed, G. U., Vogel, S. M., and Malik, A. B. (2008) *Circ. Res.* **102,** 347–355
15. Owsianik, G., Talavera, K., Voets, T., and Nilius, B. (2006) *Annu. Rev. Physiol.* **68,** 685–717
16. Schmitz, C., Perraud, A. L., Johnson, C. O., Inabe, K., Smith, M. K., Penner, R., Kurosaki, T., Fleig, A., and Scharenberg, A. M. (2003) *Cell* **114,** 191–200
17. Monteilh-Zoller, M. K., Hermosura, M. C., Nadler, M. J., Scharenberg, A. M., Penner, R., and Fleig, A. (2003) *J. Gen. Physiol.* **121,** 49–60
18. Voets, T., Nilius, B., Hoefs, S., van der Kemp, A. W., Droogmans, G., Bindels, R. J., and Hoenderop, J. G. (2004) *J. Biol. Chem.* **279,** 19–25
19. Garcia-Martinez, C., Morenilla-Palao, C., Planells-Cases, R., Merino, J. M., and Ferrer-Montiel, A. (2000) *J. Biol. Chem.* **275,** 32552–32558
20. Nilius, B., Vennekens, R., Prenen, J., Hoenderop, J. G., Droogmans, G., and Bindels, R. J. (2001) *J. Biol. Chem.* **276,** 1020–1025
21. Voets, T., Prenen, J., Vriens, J., Watanabe, H., Janssens, A., Wissenbach, U., Bodding, M., Droogmans, G., and Nilius, B. (2002) *J. Biol. Chem.* **277,** 33704–33710
22. Nilius, B., Prenen, J., Janssens, A., Owsianik, G., Wang, C., Zhu, M. X., and Voets, T. (2005) *J. Biol. Chem.* **280,** 22899–22906
23. Li, M., Du, J., Jiang, J., Ratzan, W., Su, L. T., Runnels, L. W., and Yue, L. (2007) *J. Biol. Chem.* **282,** 25817–25830
24. Mederos y Schnitzler, M., Wäring, J., Gudermann, T., and Chubanov, V. (2008) *FASEB J.* **22,** 1540–1551
25. Topala, C. N., Groenestege, W. T., Thébault, S., van den Berg, D., Nilius, B., Hoenderop, J. G., and Bindels, R. J. (2007) *Cell Calcium* **41,** 513–523
26. Oberwinkler, J., Lis, A., Giehl, K. M., Flockerzi, V., and Philipp, S. E. (2005) *J. Biol. Chem.* **280,** 22540–22548
27. Hille, B. (2001) *Ionic Channels in Excitable Membranes*, Third Ed., pp. 539–572, Sinauer Associates, Sunderland, MA
28. Sather, W. A., and McCleskey, E. W. (2003) *Annu. Rev. Physiol.* **65,** 133–159
29. Mei, Z. Z., Mao, H. J., and Jiang, L. H. (2006a) *Am. J. Physiol.* **291,** C1022–C1028

30. Mei, Z. Z., Xia, R., Beech, D. J., and Jiang, L. H. (2006b) *J. Biol. Chem.* **281,** 38748–38756
31. Hill, K., Benham, C. D., McNulty, S., and Randall, A. D. (2004) *Neuropharmacology* **47,** 450–460
32. Kraft, R., Grimm, C., Frenzel, H., and Harteneck, C. (2006) *Br. J. Pharmacol.* **148,** 264–273
33. Bo, X., Jiang, L. H., Wilson, H. L., Kim, M., Burnstock, G., Surprenant, A., and North, R. A. (2003) *Mol. Pharmacol.* **63,** 1407–1416
34. McHugh, D., Flemming, R., Xu, S. Z., Perraud, A. L., and Beech, D. J. (2003) *J. Biol. Chem.* **278,** 11002–11006
35. Starkus, J., Beck, A., Fleig, A., and Penner, R. (2007) *J. Gen. Physiol.* **130,** 427–440
36. Jung, S., Mühle, A., Schaefer, M., Strotmann, R., Schultz, G., and Plant, T. D. (2003) *J. Biol. Chem.* **278,** 3562–3571
37. Semtner, M., Schaefer, M., Pinkenburg, O., and Plant, T. D. (2007) *J. Biol. Chem.* **282,** 33868–33878
38. Jordt, S. E., Tominaga, M., and Julius, D. (2000) *Proc. Natl. Acad. Sci. U. S. A.* **97,** 8134–8139
39. Liu, D., Zhang, Z., and Liman, E. R. (2005) *J. Biol. Chem.* **280,** 20691–20699